Hyaluronic acid-based hydrogels: drug diffusion investigated by HR-MAS NMR and release kinetics

Valeria Vanoli [a,†], Sara Delleani [a,†], Mosè Casalegno [a,*], Fabio Pizzetti [a], Pooyan Makvandi [b], Havard Haugen [c], Andrea Mele [a], Filippo Rossi [a], Franca Castiglione [a,*]

[a] *Dipartimento di Chimica, Materiali e Ingegneria Chimica "G. Natta", Politecnico di Milano, via Mancinelli 7, I-20131 Milano (MI), Italy*

[b] *Istituto Italiano di Tecnologia, Centre for Materials Interfaces, viale Rinaldo Piaggio 34, 56025 Pontedera, Pisa, Italy*

[c] *Department of Biomaterials, Institute for Clinical Dentistry, University of Oslo, PO Box 1109 Blindern, NO-0317 Oslo, Norway.*

† Authors equal contribution

*** Corresponding authors**

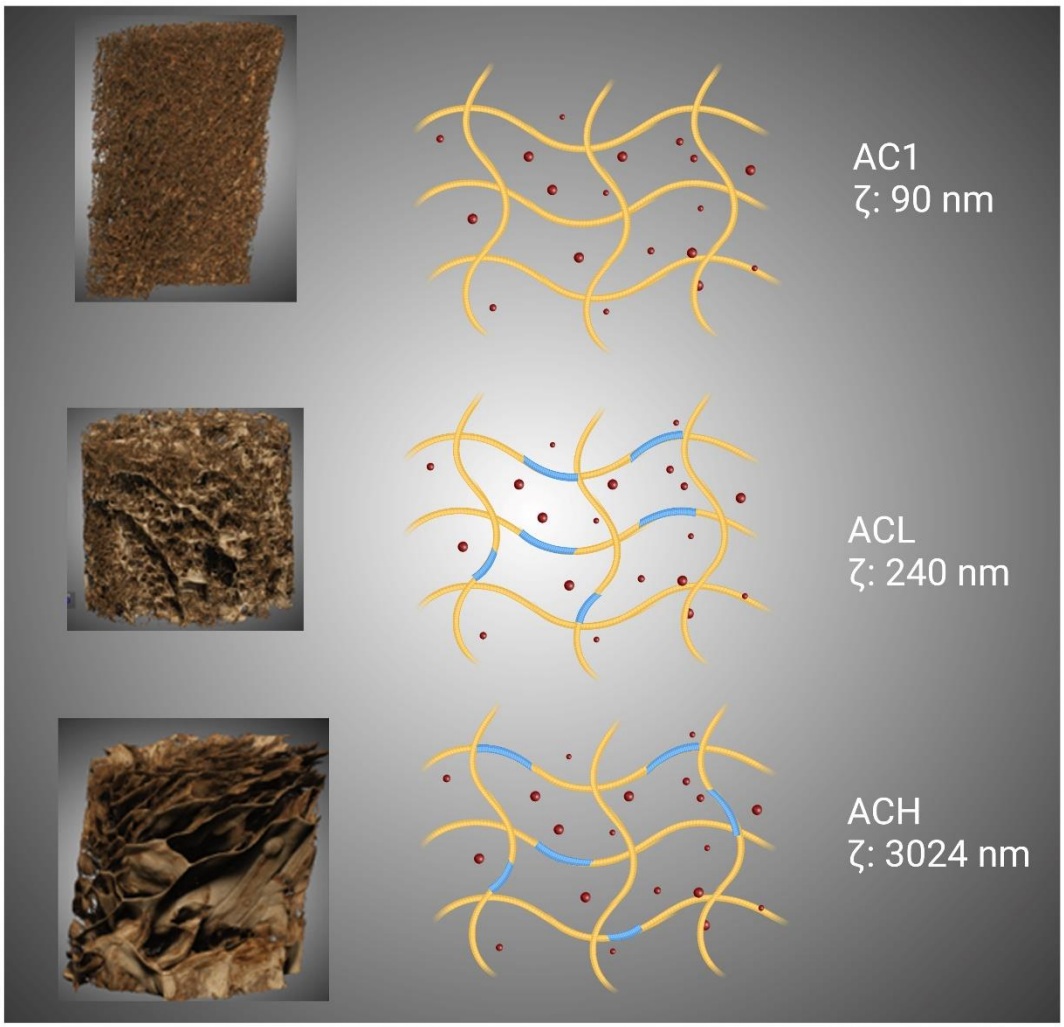

Abstract

Hydrogels based on hyaluronic acid (HA) and agarose–carbomer (AC) units have been prepared and explored as drug delivery systems. The complex architecture of the polymer network, such as mesh size, HA molecular weight and drug-polymer non-covalent interactions across the 3D polymer matrix, strongly influence the release capability/profile of these materials. In this study, High-Resolution Magic Angle Spinning (HR-MAS) NMR Spectroscopy has been used to investigate the transport behaviour of two different drugs, such as ethosuximide (neutral molecule)

and sodium salicylate (net negative charge) within the AC and AC-HA hydrogel networks prepared with different mesh sizes. Analysis of the experimental data provides evidence of superdiffusive motion for all formulations containing sodium salicylate, while ethosuximide molecules undergo unrestricted diffusion within the gel matrix. We further speculate that the superdiffusive motion observed at the nanoscale can be responsible for the faster release of sodium salicylate from all hydrogel formulations.

1. Introduction

Hydrogels based on polysaccharides of natural and synthetic origins have recently gained considerable attention in biomedical (; Yongyan et al., 2022), agricultural (Michalik, & Wandzik, 2020) and environmental (Jayakumar, Jose, & Lee, 2020) applications. Due to their versatile 3D network formed by polymer chains, cross-linked through chemical bonds or sustained by physical interactions, such as hydrogen bonds, electrostatic forces and host-guest interactions typically with cyclodextrins (Loebel, Rodell, Chen, & Burdick, 2017). Owing to their high-water contents (up to 70-99%) and soft texture, which is similar to natural living tissues, hydrogels are highly biocompatible and injectable, therefore widely employed in biomedical applications such as regenerative medicine (; Zarritaj et al., 2018; Xue, Hu, Deng, & Su, 2021) and therapeutic treatments (Hamedi, Moradi, Hudson, & Tonelli, 2018; Rial-Hermida et al., 2021; Alvarez-Lorenzo, Blanco-Fernandez, Puga, & Conceiro, 2013). As prominent drug delivery systems, hydrogels can provide controlled release profiles, and spatio/temporal release of active pharmaceutical ingredients, through appropriate release mechanisms (drug diffusion or hydrogel-matrix degradation) or, potentially, in response to externally applied stimuli, such as temperature change (Kasula, Madhusudana, Krishna, & Soo, 2022), pH (Omidi, Pirhayati, & Kakanejadifard, 2020; Kwon, Kong, & Park, 2015), magnetic field (Liao, & Huang, 2020) or physiological conditions (Ikeda, Ochi, Wada, & Hamachi, 2010). Hydrogel suitability and performance as a conventional, or "smart", drug delivery device largely depends on its bulk structure characterised by the gel mesh size, swelling degree, and the chemical composition of the macromolecules forming the polymer network. Hydrophilic polysaccharides, derived from biomass resources, such as cellulose (Chen et al., 2020), chitosan (Michalik, & Wandzik, 2020; Hamedi, Moradi, Hudson, & Tonelli, 2018; Wang et al., 2020), starch (Elvira, Mano, San Romàn, & Reis, 2002), alginate

(An, Gao, & Wang, 2020) and hyaluronic acid (Burdick, & Prestwich, 2011; Schantè, Zuber, Herlin, & Vandamme, 2011) span a wide range of molecular weight and have a polymeric backbone with diverse functional groups, e.g. hydroxyl (−OH), carboxylic (−COOH), amine (−NH2), and aldehyde (-CHO) which contribute to their diversity in structure, property and also allow them to be classified as neutral or ionic polymers. For instance, hyaluronic acid, alginate, etc., are negatively charged polysaccharides, while chitosan is positively charged (Liu et al., 2008). Among these biocompatible and biodegradable macromolecules, hyaluronic acid (HA), or hyaluronan, is a unique non-immunogenic (Laurent, 1998) biologically active biopolymer involved in various cell signalling processes (Garg, & Hales, 2004) and tissue regeneration. HA is one ideal component of hydrogels to be used in controlled release applications. Appropriate modifications of its chemical structure and properties can be addressed by adding suitable functional groups, varying the cross-linking degree and the HA molecular weight, so as to obtain hydrogels with variable stiffness, mesh size morphology and degradation rate.

sGiven these applications, understanding the mechanisms underlying drug motion inside the hydrogel network at the molecular level, the effects of the polymeric backbone (drug-polymer interactions) and its relationship with the macroscopic release is of fundamental importance for the design of efficient drug delivery systems. To date, several theoretical models have been reported, including the simple Fickian diffusion model (Tokuyama, Nakahata, & Ban, 2020), and more complex mechanistic models (Masaro, & Zu, 1999) essentially based on *i)* obstruction effects, *ii)* free volume theory (Fujita, 1961), and *iii)* hydrodynamic theories (Cukier, 1984) which consider the hydrodynamic interactions present in the whole system. Furthermore, a comprehensive multi-scale model, accounting for the effects of different diffusion mechanisms, has been proposed to describe the diffusion of dextran of different sizes in a series of poly(ethylene

glycol) (PEG) and alginate-based hydrogels (Axpe et al., 2019). Despite these advancements, considering the effect on the diffusion motion of non-covalent drug-polymer chemical interactions and their connection with macroscopic properties is still a challenging task. In a previous work (Castiglione et al., 2019) we applied the continuum random walk theory (CRWT) (Metzler, & Klafter, 2000) to describe the anomalous superdiffusive motion of ibuprofen in agarose-carbomer hydrogels with variable mesh size and drug concentration. There, hydrogen bonds formation and dissociation were identified as the main factor responsible for the observed Lèvy flight solute dynamics (Viswanathan et al., 1996; Blumen, Zumofen, & Klafter, 1989; Song, Moon, Jeon, & Park, 2018).

Experimentally, many techniques are available to investigate particle dynamics, such as single-particle tracking (Serag, Abadi, & Habuchi, 2014; Kusumi et al., 2014), refractive index methods (Liang et al., 2006) and fluorescence correlation spectroscopy used by Zustiak and coworkers to probe molecular diffusion in crosslinked PEG-based networks (Zustiak, Boukari, & Leach, 2010). Nuclear magnetic resonance spectroscopy (NMR) also provides a powerful way to investigate molecular motion in a non-invasive way on a millisecond time-scale, using pulse gradients spin echo (PGSE) methodologies (Johnson, 1999; Zubkov et al., 2016). These methods, along with the High-Resolution Magic Angle Spinning (HR-MAS) setting, were used to study the diffusion motion in hydrogels (Ferro et al., 2014; Alam, Childress, Pastoor, & Rice, 2014), polymers (Jenkins, Hibbs, & Alam, 2012) and other semi-solid materials (Pivato et al., 2021).

In this work, we use the HR-MAS PGSE NMR techniques to characterise the diffusion of ethosuximide and sodium salicylate loaded in hyaluronic acid-agarose-carbomer hydrogels with different mesh sizes, prepared according to the procedure described by Pizzetti et al. (Pizzetti, Maspes, Rossetti, & Rossi, 2021). The aim of this work is to determine how the drug diffusion

motion is affected by the nanostructured 3D polymer network, drug-polymer interactions and drug concentration. The NMR results will be compared with the macroscopic *in vitro* release kinetics.

2. Materials and methods

2.1 Materials

The polymers used are Carbomer 974P MW=1 MDa, by Fagron (The Netherlands) and Agarose MW = 200 kDa, by Invitrogen Corp. Three different types of hyaluronic acids, purchased from Lifecore Biomedical (USA), sodium hyaluronate 10 K (MW = 10 kDa), sodium hyaluronate 40 K (MW = 40 kDa), sodium hyaluronate 1 M (MW = 1 MDa) were used. The drugs were sodium salicylate and ethosuximide, purchased from Sigma-Aldrich (Germany). Deuterium oxide (99.9 % deuterium content) was provided by Sigma-Aldrich, Germany. All materials were used as received.

2.2 Hydrogel synthesis and drug loading

In this work, two different hydrogels were investigated, one based on agarose-carbomer (AC) only and one AC modified by the addition of hyaluronic acid (HA). A reference formulation, hereafter AC1, was prepared as follows. 0.05 g of carbomer 974P were stirred in deuterated PBS buffer (10 mL). Agarose powder (0.5% w/v) was subsequently added and the system was electromagnetically heated up to 80°C to induce condensation reactions. The gelling solutions were then placed in steel cylinders at 37°C until complete gelation occurred. The chemical processes involving forming ester bonds between agarose and carbomer during the reaction have been described previously (Perale et al., 2011).

Starting from the AC1 formulation, new samples were prepared by adding a variable amount of hyaluronic acid. The process (Pizzetti, Maspes, Rossetti, & Rossi, 2021) involves the replacement of a fraction of the carbomer in the AC1 gel with low (MW = 104 g/mol) or high (MW = 106 g/mol) molecular weight hyaluronic acid in different proportions, in particular, two thirds (2/3, 67%) for low molecular weight (formulation L) and one third (1/3, 33%) for high molecular weight (formulation H). This choice was based on the final morphological yield, which was better for the reported proportions. The synthesis of these new formulations, once defined the type of hyaluronic acid to use was similar to that of the reference hydrogel AC1. For this work, three mesh sizes were chosen: AC1 (90 nm), ACL (240 nm) and ACH (3024 nm). The hydrogel's chemical structure and mesh sizes are reported in Scheme 1 and Figure 1.

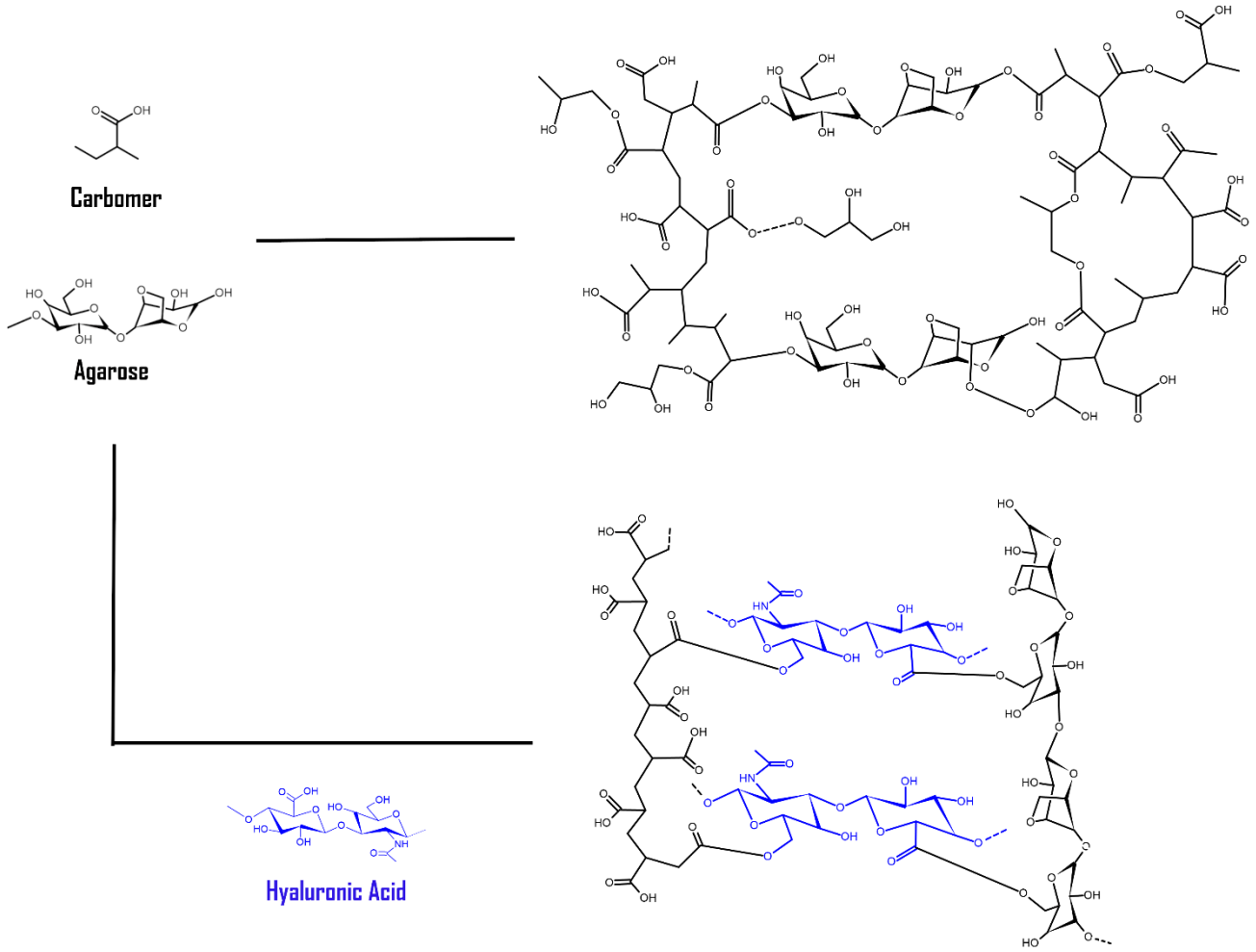

Scheme 1. Schematic representation of the chemical structures of: a) AC1 hydrogel b) ACH and ACL hydrogels.

Ethosuximide and Sodium Salicylate were selected as loading drugs, being both small molecules but with two different charges: the former has no net charge, while the latter has a negative charge. The chemical structure of both drugs is displayed in scheme 2.

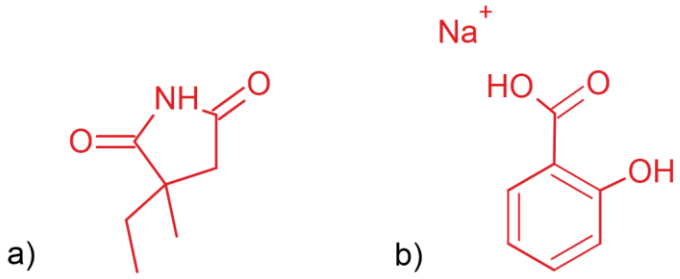

Scheme 2. Chemical structure of the drugs: a) ethosuximide, b) sodium salicylate.

Both drugs were added to the polymeric formulation as aqueous solutions, before the cross-linking procedure, and thus sol/gel transition occurred. Each drug was loaded in two different concentrations: 40 mg/ml and 80 mg/ml for HR-MAS NMR samples.

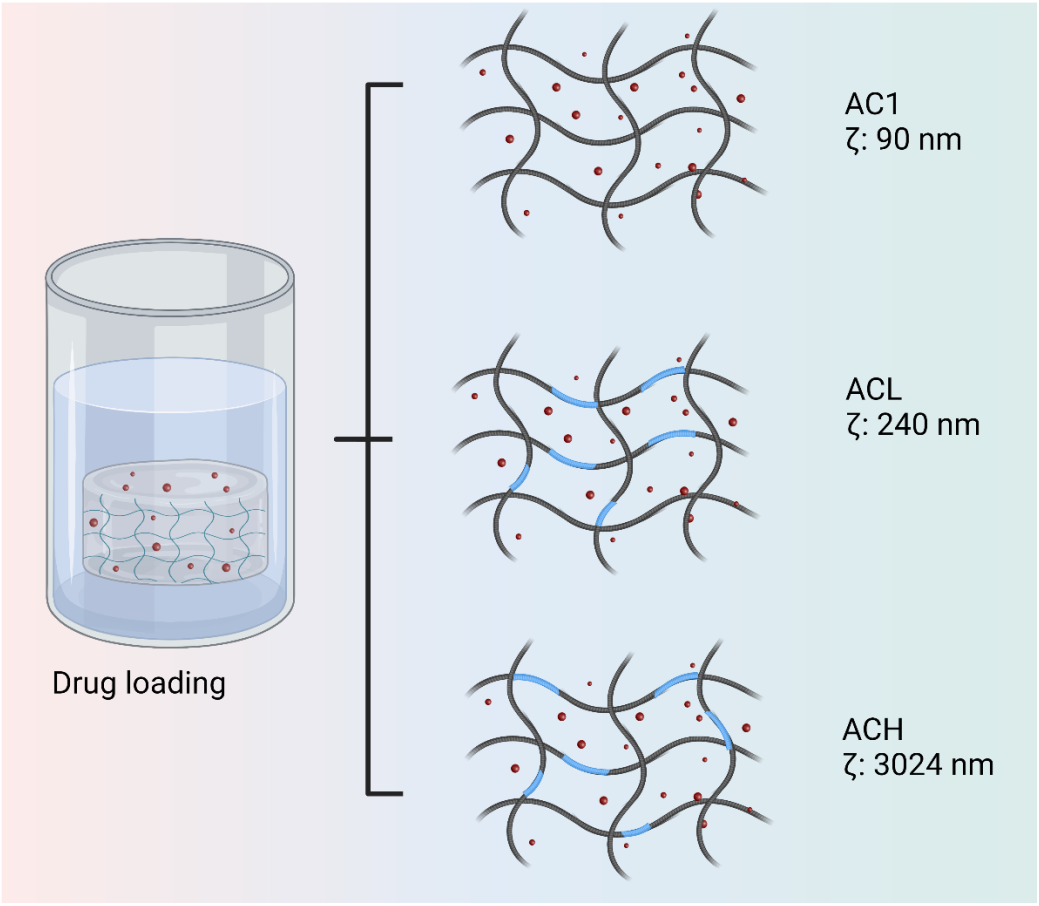

Fig. 1. Sketch of the AC1, ACL and ACH hydrogels mesh size and drug loading.

2.3 In vitro release studies

Three gel samples loaded with a drug concentration of 5 mg/mL were prepared. The samples were submerged in 2 mL of PBS (0.1 M, pH 7.4) and stored at 37°C under a 5% CO_2 atmosphere. Minimal aliquots (1000 µL of the released media) were collected at defined time points in the range (5 min-144 h) while the solution was refreshed to avoid mass-transfer equilibrium between the gel and the surrounding PBS solution. The amount of drug released was measured spectrophotometrically at the wavelength corresponding to the absorbance peak (Ethosuximide= 244 nm, Sodium salicylate 236 nm) and determined by referring to the standard calibration curve for each of them. Each measurement was repeated in triplicate.

2.4 FT-IR Spectroscopy

Infrared (IR) spectra were recorded using a Varian 640-IR spectrometer from Agilent Technologies, using the ATR (attenuated total reflection) technique. Spectra were collected at room temperature under a dry nitrogen atmosphere in the 400-4000 cm^{-1} wavenumber range. Measurements were made on freeze-dried hydrogel samples.

2.5 Nano-computed tomography

All samples were scanned in a nano-computed tomography (nano-CT) device (SkyScan 2211 Multiscale X-ray Nano-CT System, Bruker micro-CT, Kontich, Belgium) with a 20–190 kV tungsten X-ray source and a dual detection system: an 11-megapixel cooled 4,032 x 2,670-pixel

CCD-camera and a 3-megapixel 1,920 x 1,536 pixel CMOS flat panel. Prepared roots for cementum analysis were scanned at 38 kV, 370 μA and 1400 ms. The scans were taken over 180º with a rotation step of 0.14° and a voxel size of 800 nm using the CCD detector. Projections were reconstructed using the system-provided software, NRecon (version 1.7.4.6), and analysed with CTAn (Bruker micro-CT, version 1.18.4.0).

2.6 NMR Spectroscopy

The ^{1}H HR-MAS spectra of every hydrogel systems were recorded using a Bruker Avance DRX spectrometer operating at 500 MHz proton frequency, equipped with a dual $^{1}H/^{13}C$ high-resolution magic angle spinning (HR-MAS) probe head for semi-solid samples. This approach relies on the fast rotation of the sample at the so-called magic angle (54.7° with respect to the z direction of the stray field of the NMR magnet), which averages the dipole–dipole interactions and susceptibility distortions, allowing to record spectra with a solution-like resolution. Samples were transferred in a 4 mm ZrO_2 rotor containing a volume of about 12 μL. The temperature was set and controlled at 305 K with an air flow of 535 $L \cdot h^{-1}$ to avoid any temperature fluctuations due to sample heating during the magnetic-field pulse gradients. All the ^{1}H NMR spectra were acquired with a spinning rate of 4 kHz.

Self-diffusion coefficients were measured using PGSE methods. A pulsed gradient unit was used to produce magnetic-field pulse gradients in the z direction up to 53 G·cm-1. These experiments were performed using the bipolar pulse longitudinal eddy current delay (BPPLED) pulse sequence. The duration of the magnetic-field pulse gradients (δ) and the diffusion times (Δ) were optimised for each sample to obtain complete dephasing of the signals with the maximum gradient strength. For the investigated samples, Δ varied from 0.01s to 0.2s, while the δ values varied in the range of

0.5-3ms. Each experiment collected a series of 40 spectra with 32K points. The pulse gradients were increased linearly from 2 to 95% of the maximum gradient strength.

2.7 PGSE-NMR theory and data modelling

PGSE-NMR spectroscopy encodes the spatial position of molecules by employing pulsed magnetic field gradients of varying intensity. At t = 0, the probe molecules are labelled by the pulsed field gradient according to their position. After diffusion has occurred over a specific time t, the observed signal intensity *I(q,t)* is attenuated according to the following general relationship:

$$I(\mathrm{q,t})=\mathrm{I}(0,\mathrm{t})\cdot e^{\frac{-1}{2}q^2\langle z^2(t)\rangle} \quad (1)$$

where q is the reciprocal space coordinate, defined as q = (δγg)/2π, γ is the magnetogyric ratio of the observed nucleus, g is the field gradient, δ is the gradient pulse and $\langle z^2(t)\rangle$ represents the mean squared displacement (MSD).

The signal decay is related to the corresponding displacement probability distribution, *G(z,t)* by means of the following relationship (Cohen, & Assaf, 2002):

$$I(\mathrm{q,t}) = \int_{-\infty}^{+\infty} G\,(\mathrm{z,t})\cdot e^{-\mathrm{iqz}}\mathrm{dz} \quad (2)$$

Assuming G(z,t) a normalised Gaussian containing the self-diffusion coefficient D, e.g.:

$$G(\mathrm{z,t})=\mathrm{I}(0,\mathrm{t})\cdot\sqrt{\frac{\pi}{\mathrm{Dt}}}\cdot e^{\frac{-z^2}{4\mathrm{Dt}}} \quad (3)$$

Eq. (4) is finally obtained:

$$I(\mathrm{q,t})=\mathrm{I}(0,\mathrm{t})\cdot e^{-\mathrm{Dt}q^2} \quad (4)$$

In common NMR practice, Eq. (5) is often used by taking the natural logarithm of the normalised signal intensity as follows:

$$ln\frac{I(\mathrm{q,t})}{I(0,\mathrm{t})} = -q^2\mathrm{Dt} \quad (5)$$

The linear relationship between ln (I/I_0) and q^2 suggests a simple way to determine the diffusion coefficient via simple linear regression, which is the method currently adopted in routine NMR data analysis. Eq. (5) holds in the case G(z,t) is gaussian (Eq. (3)), which also implies that the MSD varies linearly in time. This can be seen by comparing Eqs. (1) and (4), to obtain:

$$\langle z^2(t) \rangle = 2Dt \quad (6)$$

The linear relationship between MSD and time is often referred to as Fickian diffusion, after the Fick's laws of diffusion (Fick, 1855). Species diffusing in a homogeneous isotropic medium follow Fickian and Gaussian diffusion. This kind of diffusion is often called "ordinary", to distinguish it from "anomalous" diffusion, a term used to group many situations where the MSD grows non-linearly in time. The following general expression is often used to describe either ordinary or anomalous diffusion:

$$\langle z^2(t) \rangle \sim t^{\alpha} \quad (7)$$

where α is the diffusion exponent. When α = 1, Eq. (7) reduces to the Fickian case, whereas species not following a Fickian diffusive behaviour may be expected to show values of α different from one, thereby corresponding to subdiffusion ($0 < \alpha < 1$) or superdiffusion ($\alpha > 1$).

It should be noted that deviations from a Gaussian displacement distribution function do not necessarily imply deviations from the Fick's law. Although not ubiquitous (Cuetos, Morillo, & Patti, 2018), several examples have been reported where the diffusion is Fickian and not Gaussian in soft and biological systems (Wang, Kuo, Bae, & Granick, 2012; Wang, Anthony, Sung, & Granick, 2009; Lutsko, & Boon, 2013; Di Meo, Coviello, Matricardi, & Lamanna 2021). The occurrence of anomalous diffusion in such systems may be linked to the system's inhomogeneities. Structurally heterogeneous systems, such as hydrogels, may represent ideal media where anomalous diffusion occurs (Malgaretti, Pagonabarraga, & Miguel Rubi, 2016).

This prompted us to develop a general method (Castiglione et al., 2019) that could be used to extract the value of α from PGSE-NMR data, thereby bypassing the limitations posed by the conventional approach, exemplified by Eq. (5). In the present work, we further develop this method, making an additional step towards a more precise determination of α.

As a starting point to describe our approach, we consider one important property of *G(z,t)*, known as self-similarity (Metzler, & Klafter, 2000; Sagi, Brook, Almog, & Davidson, 2012). As shown in our previous work (Castiglione et al., 2019), the displacement distribution associated with a set of diffusion times, hence with a single PGSE-NMR experiment, can be expected to scale in time and space as:

$$t_1^{-\alpha/2} G\left(z \cdot t_1^{-\alpha/2}, \mathrm{t}_1\right) = t_2^{-\alpha/2} G\left(q \cdot t_2^{-\alpha/2}, \mathrm{t}_2\right) \quad (8)$$

where t_1 and t_2 are any two diffusion times.

In our previous work, we used Eq. (8) to determine the value of α from the displacement distributions obtained by Fourier transforming the corresponding NMR signal intensities. Although this approach proved reliable, the reconstructed *G(z,t)* showed spurious oscillations related to a finite q-space interval sampling.

In order to circumvent this issue, we started from Eq. (8) to develop a scaling property for the NMR signal intensities. The demonstration, available in the SI, can be stated as follows:

$$I\left(q \cdot t_1^{\alpha/2}, \mathrm{t}_1\right) = \mathrm{I}\left(q \cdot t_2^{\alpha/2}, \mathrm{t}_2\right) \quad (9)$$

Eq. (9) implies that, for an appropriate choice of α, all intensity profiles should collapse onto a unique curve, which is often referred to as the "master" curve (Sagi, Brook, Almog, & Davidson, 2012). The master curve can simply be obtained by scaling the abscissae (q values) of all the intensities obtained at different diffusion times (t_1, t_2, t_3...) by means of the corresponding scaling factors: $t_1^{\alpha/2}, t_2^{\alpha/2}, t_3^{\alpha/2}$...

This approach, from now on referred to as *q-scaling*, does not require explicit knowledge of the displacement distribution functions, thus providing a simple way to access the value of α from unprocessed NMR data.

To illustrate this concept further, in Figure 2 the ^{1}H NMR signal intensities for a water sample as raw data and reported after q-scaling with α values between 0.6 and 1.4. As expected for bulk water, setting α = 1 brings the profiles closer to each other than any other value. It should be noted, that the precise numerical determination of α, from NMR data processing, may depend on experimental factors such as sample quality, signal noise, and others.

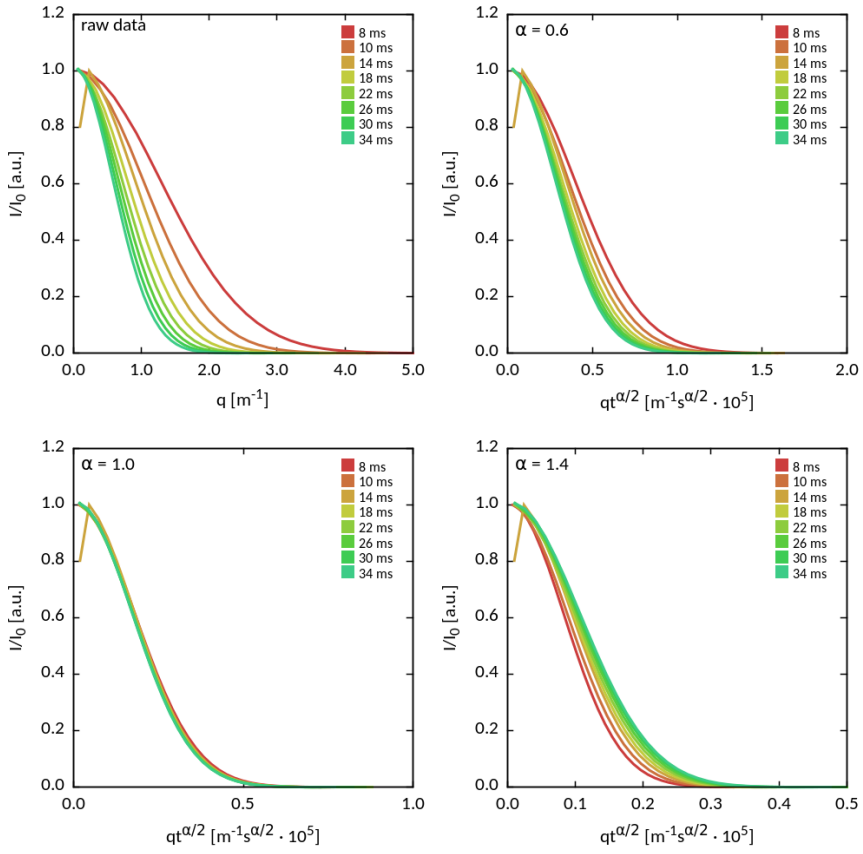

Fig. 2. PGSE-NMR normalised signal intensities as a function of q, for a water sample between 8 and 34 ms. Top left: raw data. The remaining panels display the intensity profiles rescaled by $t^{\alpha/2}$, with α = 0.6, 1.0, and 1.4, respectively.

Once the value of α has been determined, a functional form for I(q,t) is necessary to capture the relationship between signal intensity and the diffusion coefficient. According to our previous work (Castiglione et al., 2019), we chose the following:

$$\mathrm{I(q,t)} = \mathrm{I(0,t)} \cdot e^{-Kt^{\beta}q^{\mu}}, \tag{10}$$

where K is a generalized diffusion coefficient with dimensions $\left[m^{\mu}s^{-\beta}\right]$. The exponents β and μ are related to α by means of the following equation:

$$\alpha = \frac{2\beta}{\mu}. \tag{11}$$

A brief comment on the physical meaning of β and μ will be given in Section 3.3. As previously noted, (Castiglione et al., 2019) Eq. (10) is not rigorously derived from a generalised solution of the fractional diffusion equation (Metzler, & Klafter, 2000), except for some limiting cases which, however, are frequently encountered, namely subdiffusion (α < 1, μ = 2, 0 < β < 1) for $q^2 \ll 1/Kt^{\beta}$ (Capuani et al., 2013; Palombo et al., 2011; Palombo et al., 2022) and superdiffusion (α > 1, μ < 2) for β = 1 (Yang, Reutens, & Vegh, 2022). Its adoption is further justified by the fact it recovers Eq. (4) for ordinary diffusion (α = 1, μ = 2), and based on previously reported NMR studies on anomalous diffusion (Capuani et al., 2013; Palombo et al., 2011; Palombo et al. 2022; Yang, Reutens, & Vegh, 2022; Lin, 2017). Finally, we note that it conforms to the scaling property outlined above (i.e. Eq.(9)), through the substitution $t^{\beta}q^{\mu} = \left(qt^{\alpha/2}\right)^{\mu}$. We shall return to the choice of this functional form below. Once the value of α has been determined, the parameters K and μ (or β) can be obtained, fitting the master curve. In this work, the fitting of such parameters was addressed utilizing the Levenberg-Marquardt method (Levenberg, & Kenneth, 1944), whereas

a different strategy was adopted for fitting α. Further details about the numerical implementation of this procedure are provided in the SI.

2 Results and discussion

3.1 IR Spectroscopy

FT-IR spectroscopy confirmed the structure of AC1 and AC-hyaluronic acid hydrogels loaded with ethosuximide and sodium salicylate drugs. All spectra acquired in the region 500-4000 cm^{-1}, show similar features and are displayed in Figure 3. The broad band observed at 3000–3500 cm^{-1} corresponds to the O–H stretching groups. The peaks at 2977 cm^{-1} and 2898 cm^{-1} are attributed to C-H stretching vibration. The C=O stretching vibrations are observed at 1712 cm^{-1} and the peaks at 1405-1570 cm^{-1} are due to the presence of stretching vibration of COO^- ions.

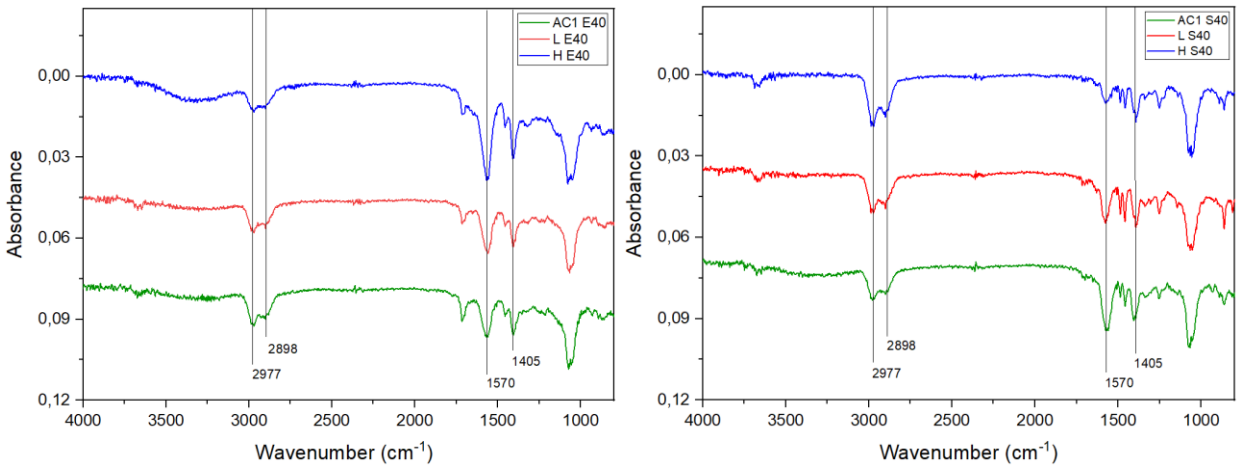

Fig. 3. Fourier transform infrared (FT-IR) spectra (500-4000 cm^{-1} region) of AC1, ACL and ACH hydrogels loaded with ethosuximide (*left panel*) and sodium salicylate (*right panel*).

3.2 NanoCT

Morphology characterisation of the porous structure of the synthesised hydrogel was conducted with nano-CT technology that allowed us to obtain a 3D reconstruction of the sample's internal

structure and evaluate the porosity of the system. Figure 4 shows the reconstruction of the sample where the porosity of the system and their interconnection can be observed (details in Supporting Information). The presence of the two phases is visible from the two colours representing the polymeric phase (light colour) and water phase (dark colour). About open porosity, the amount of interconnected pores that create a continuous porous system is higher than 95% in all the samples analysed.

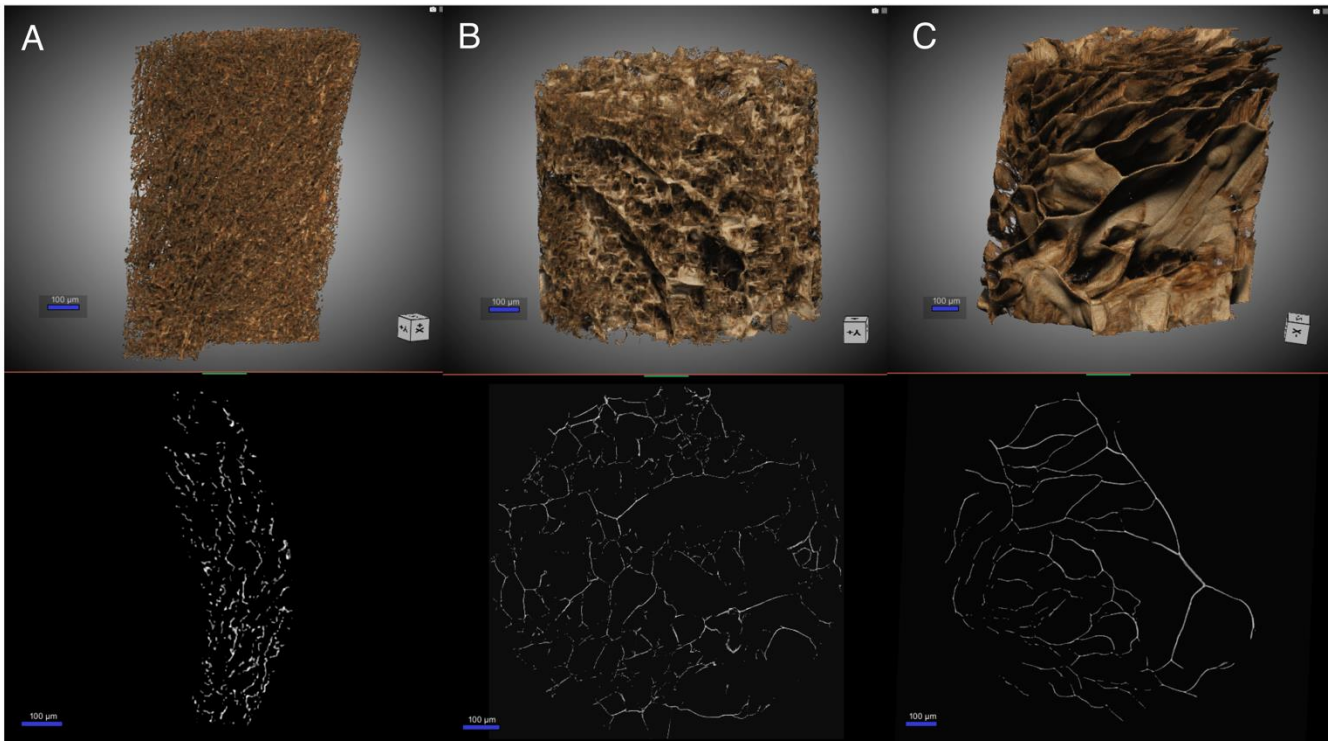

Fig. 4. NanoCT images of the hydrogels synthesised: AC1 (A), ACL (B) and ACH (C) (scale bar = 1 μm).

3.3 HR-MAS NMR measurements

We begin our investigation considering the results obtained for ethosuximide-loaded hydrogels. These will be labelled with the prefixes E40 and E80, corresponding to 40 and 80 mg/ml, respectively. For comparison, NMR data were also collected for the corresponding ethosuximide water solutions, called E40-WAT and E80-WAT.

Table 1. Numerical values of α, μ, β, and K were calculated by fitting the NMR data of ethosuximide samples (40 mg/mL) in water (E40-WAT) and hydrogels. The diffusion coefficients, D, obtained according to the standard regression (α = 1 and μ = 2) are also reported.

Sample	α	μ	β	K [m^{μ}/s^{β}]	D [m^2/s]
E40-WAT	1.074(31)	1.950(3)	1.050(31)	$1.60(6) \cdot 10^{-9}$	$0.819(6) \cdot 10^{-9}$
E40-AC1	1.037(9)	1.910(5)	0.991(10)	$2.91(17) \cdot 10^{-9}$	$1.063(10) \cdot 10^{-9}$
E40-ACL	1.134(4)	1.800(9)	1.020(6)	$1.16(11) \cdot 10^{-8}$	$1.170(35) \cdot 10^{-9}$
E40-ACH	1.065(13)	1.830(10)	0.973(13)	$7.41(78) \cdot 10^{-9}$	$1.079(20) \cdot 10^{-9}$

Table 1 collects the diffusion parameters (α, μ, β, and K) obtained by fitting the NMR signal intensities for E40. The diffusion coefficients (D) obtained with the standard regression model (Eq. (6)) are also reported. The diffusion of ethosuximide in the water quite closely approaches ordinary diffusion (α = 1 and μ = 2), as indicated by the values of the parameters α and μ. The plots of the signal intensities and the master curves obtained employing the two methods, compared in the SI (Figure S3.1), confirm this conclusion. In both cases the fitting procedure yielded comparably good results, closely approaching the experimental data. The master curve resulting from the optimisation of α (panel D) and described in the previous section (see above),

slightly better describes the data than assuming $\alpha = 1$. The diffusion coefficient for the standard regression model in water ($D = (0.819 \cdot 10^{-9} \pm 5.88 \cdot 10^{-12})$ m^2/s) turned out to be smaller than the corresponding value of K ($1.60 \cdot 10^{-9} \pm 5.74 \cdot 10^{-12}$) m^{μ}/s^{β}). We note, however, that the two coefficients can only be compared qualitatively due to the different units. The value of the generalised diffusion coefficient can be sensitive to the values of α and μ (or β), which is reasonable, considering the functional form of Eq. (10).

Ongoing from water to the hydrogel samples, some small deviations from unrestricted diffusion were observed, as suggested by the value of μ, whereas the value of α remained essentially unaltered. Furthermore, the statistical uncertainties of the diffusion coefficients of ethosuximide were larger than those estimated in water. This outcome, in line with the estimates reported in our previous work (Castiglione et al., 2019), was due to a natural increase of in signal noise brought about by the surrounding gel environment. The effect of sample heterogeneity on data collection can be fully appreciated in Figure 5, where the results obtained for E40-ACL, by means of both approaches, are compared by means of both approaches. Overall, use of Eq. (10) better described signal attenuation profiles than the standard diffusion model. Similar results were obtained for AC1 and ACH samples (reported in the SI), thereby confirming the need to generalise the Gaussian diffusion model when modelling drug diffusion in hydrogels.

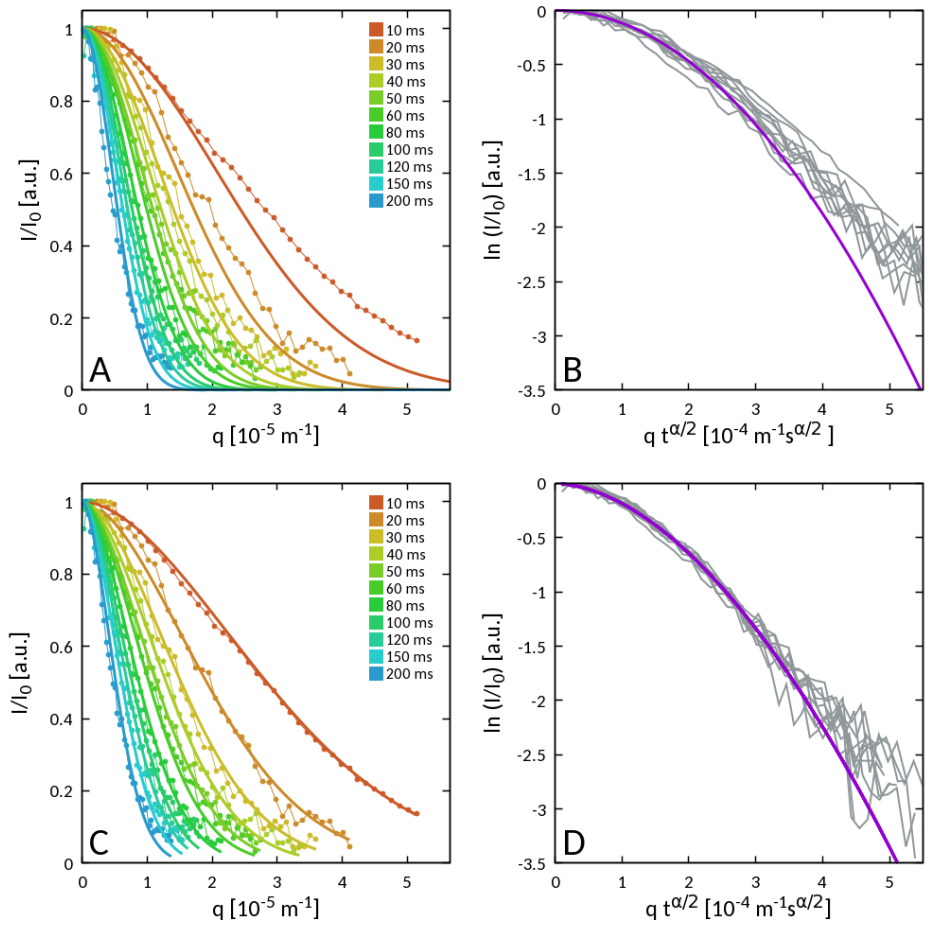

Fig. 5. NMR signal intensities (left) corresponding master curves (right) for E40-ACL. Top panels (A, B): results obtained fitting the data via linear regression (see Eq.(5)). Bottom panels (C, D): results obtained fitting the data via Eqs. (10) and (11).

Our results for E80 samples are collected in Table 2. Again, the fitting parameters for ethosuximide diffusing in water quite closely matched those of ordinary diffusion.

In line with the previous results for E40 samples, hydrogel-loaded samples showed mild changes in α and a moderate decrease in μ, for all of the polymer matrices. the value of β was quite close to unity. As for E40, the sample with the largest deviations from ordinary diffusion was ACL. Figure 6 compares the results obtained by means ofutilizing standard regression and our model for the E80-ACL sample (similar plots are available in the SI for the other samples). The comparison

betweenComparing the master curves (panels B and D) indicates that the optimisation of α is necessary to fit the signal intensities accurately. At the same time, considering our experimental data's accuracy and the investigated concentrations, these values do not provide unequivocal evidence of anomalous diffusion for ethosuximide. Overall, the diffusion of ethosuximide in hydrogels appears to be essentially unrestricted and closely similar to that observed in water. Therefore, we shall briefly return to this point below.

Table 2. Numerical values of α, μ, β, and K calculated by fitting the NMR data of ethosuximide samples (80 mg/mL) in water (E80-WAT) and hydrogels. The diffusion coefficients, D, obtained according to standard regression (α = 1 and μ = 2) are also reported.

Sample	α	μ	β	K [m^{μ}/s^{β}]	D [m^2/s]
E80-WAT	1.045(38)	1.995(1)	1.043(38)	$8.69(10) \cdot 10^{-10}$	$0.739(8) \cdot 10^{-9}$
E80-AC1	1.069(10)	1.837(7)	0.982(10)	$6.53(48) \cdot 10^{-9}$	$1.057(19) \cdot 10^{-9}$
E80-ACL	1.154(15)	1.759(9)	1.015(15)	$2.00(18) \cdot 10^{-8}$	$1.211(39) \cdot 10^{-9}$
E80-ACH	1.041(15)	1.805(16)	0.940(16)	$7.30(12) \cdot 10^{-9}$	$8.919\ (12) \cdot 10^{-10}$

Meanwhile, we note that this conclusion is consistent with the results of our previous study (Rossi et al., 2015), where the ethosuximide diffusion in AC1 hydrogels was investigated according to the ordinary diffusion model. In that case, we were able to observe a concentration-dependent behaviour of the diffusion coefficient due to the adsorption of drug molecules into the pores of the hydrogel matrix.

This phenomenon was found to affect ethosuximide diffusion in AC1 only at low concentrations (~ 4 mg/mL), whereas the unrestricted diffusion regime was restored at higher concentrations (> 19 mg/mL), due to pore saturation. The estimates herein reported for the diffusion coefficients obtained via standard regression in water (E40-WAT and E80-WAT) and AC1 (E40-AC1 and E80-AC1) (see Tables 1 and 2) are in line with our previous findings. However, due to the increase in solute concentration, the diffusion coefficient of E80-WAT is lower than that of E40-WAT. In AC1, conversely, similar values were found, regardless of ethosuximide concentration.

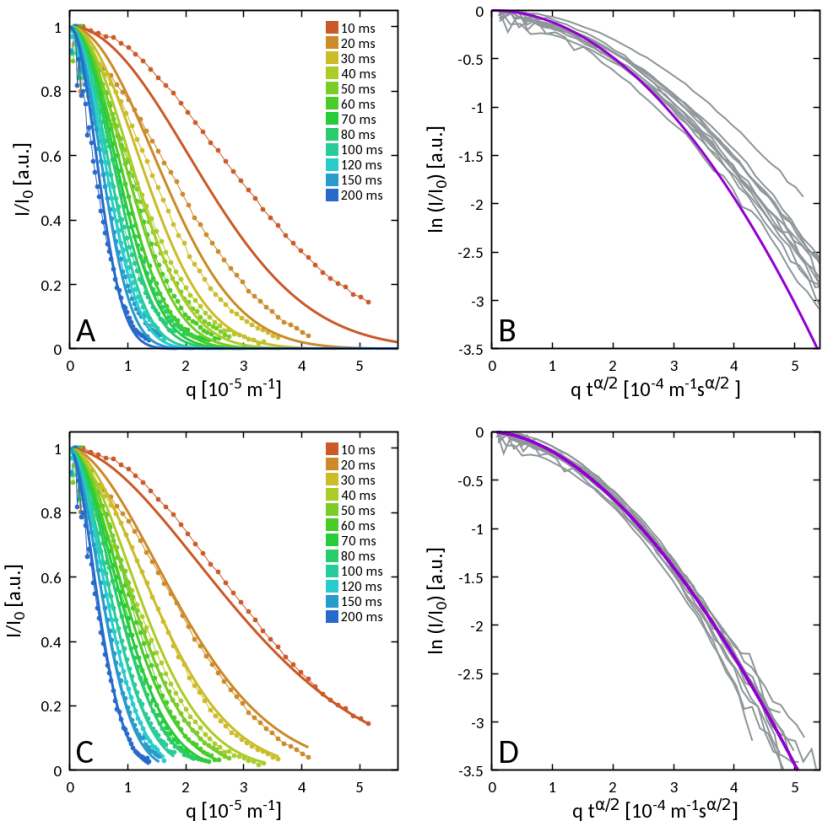

Fig. 6. NMR signal intensities (left) corresponding master curves (right) for E80-ACL. Top panels (A, B): results obtained fitting the data via linear regression (see Eq. (5)). Bottom panels (C, D): results obtained fitting the data via Eqs. (10) and (11).

As shown by our results, the modification of the hydrogel network, induced by the reaction with the hyaluronic acid, did not substantially affect ethosuximide diffusion, except for the ACL sample, for which our results suggest a mild superdiffusive behaviour. On the molecular scale, the drug-hydrogel interactions can be rationalised considering the formation of hydrogen bonds between ethosuximide and carbomer-agarose units. Such interactions may be responsible for the physical adsorption of ethosuximide by the hydrogel, and the concentration-dependent behaviour mentioned above. Similar interactions may also occur between ethosuximide and hyaluronic acid units, so we may reasonably expect pore saturation to also occur in ACL and ACH hydrogels. Furthermore, the way drug-polymer interactions may affect ethosuximide diffusion in these systems is challenging to quantify, and further investigations will be necessary to understand better the results here obtained for ACL.

On the physical side, we may reasonably exclude this difference related to the size of the hydrogel matrix pores. Indeed, the mean hydrodynamic radius of ethosuximide (~0.76 nm) is too small concerning the average mesh size of the hydrogels to justify the onset of pore-mediated diffusion. The data for the samples S40 and S80 of salicylic acid are reported in Table 3 and 4 respectively. In this case, the values reported also refer to the diffusion parameters obtained by means ofusing the two approaches considered here. Our results indicate that the diffusion of salicylate in water closely approaches ordinary diffusion. This conclusion is clearly supported by the values of α and μ obtained in both samples.

By contrast, salicylate-loaded hydrogels show a different outcome, characterised by values of α in the range 1.2-1.4 and values of μ in the range 1.5-1.8, hence falling in the superdiffusive regime (see above). The difference between ordinary and anomalous diffusion clearly emerges by

comparing the results for S40-ACL reported in Figure 7. Analogous results were obtained for the other S40 and S80 samples (see the SI).

Table 3. Numerical values of α, μ, β, and K were calculated by fitting the NMR data of sodium salicylate samples (40 mg/mL) in water (S40-WAT) and hydrogels. The diffusion coefficients, D, obtained according to the standard regression (α = 1 and μ = 2) are also reported.

Sample	α	μ	β	K [m^{μ}/s^{β}]	D[m^2/s]
S40-WAT	1.066(36)	2.004(2)	1.068(36)	$7.83(13) \cdot 10^{-10}$	$7.056(34) \cdot 10^{-10}$
S40-AC1	1.394(16)	1.388(8)	0.968(10)	$1.54(15) \cdot 10^{-6}$	$2.156(135) \cdot 10^{-9}$
S40-ACL	1.257(34)	1.564(3)	0.983(19)	$2.50(17) \cdot 10^{-7}$	$2.208(93) \cdot 10^{-9}$
S40-ACH	1.225(20)	1.621(6)	0.993(12)	$9.51(91) \cdot 10^{-8}$	$1.249(29) \cdot 10^{-9}$

Table 4. Numerical values of α, μ, β, and K were calculated by fitting the NMR data of sodium salicylate samples (80 mg/mL) in water (S80-WAT) and hydrogels. The diffusion coefficients, D, obtained according to the standard regression (α = 1 and μ = 2) are also reported.

Sample	α	μ	β	K [m^{μ}/s^{β}]	D[m^2/s]
S80-WAT	1.068(36)	2.005(1)	1.071(36)	$7.03(94) \cdot 10^{-10}$	$6.370(39) \cdot 10^{-10}$
S80-AC1	1.327(05)	1.777(8)	1.179(07)	$4.07(30) \cdot 10^{-8}$	$2.506(117) \cdot 10^{-9}$
S80-ACL	1.251(05)	1.709(4)	1.069(05)	$5.39(22) \cdot 10^{-8}$	$1.860(54) \cdot 10^{-9}$
S80-ACH	1.324(06)	1.509(6)	0.999(06)	$5.25(31) \cdot 10^{-7}$	$2.480(117) \cdot 10^{-9}$

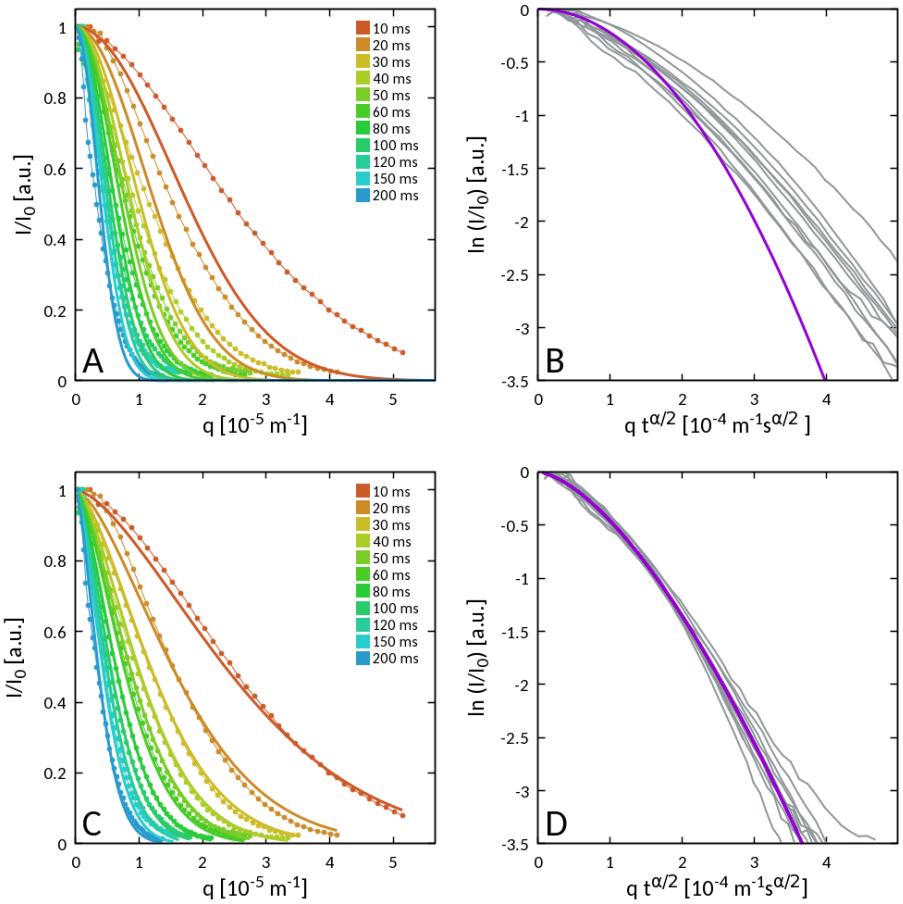

Fig. 7. NMR signal intensities (left) corresponding master curves (right) for S40-ACL. Top panels (A, B): results obtained fitting the data via linear regression (see Eq.(5)). Bottom panels (C, D): results obtained fitting the data via Eqs. (10) and (11).

The inspection of α values reported in Tables 3 and 4 does not reveal a clear, systematic trend across salicylate concentrations nor hydrogel composition. However, the larger values found in AC1 samples are plausibly due to the numerical fluctuations in the corresponding NMR data (see the SI).

In any case, for all the data considered, our findings provide quite a strong evidence of superdiffusive transport for salicylate, characterised by $\alpha > 1$. This result is different to that found for ethosuximide, where, although greater than unity, the value of α was close to that found in water.

At this point, it is worth resuming some of the fundamental concepts behind adopting Eq. (10), used in modelling our data. As mentioned above, this equation represents a special case of the more general solution of the fractional diffusion equation, developed in the context of the continuous time random walk theory (CTRW) (Metzler, & Klafter, 2000). According to this theory, the molecules diffuse with displacement probability distributions whose functional dependence on time and space are governed by the values of β and μ, respectively. These parameters can be better rationalised thinking of molecular diffusion as the motion of walkers randomly jumping from one site to another in a hindered and heterogeneous medium. The value of β can be associated with the time elapsed between consecutive jumps. The necessity to follow a given path within the medium may increase this waiting time, eventually leading to subdiffusion. The value of μ can be associated with the jump length, e.g. the spatial part of the probability distribution. Long tails in the probability distribution, reflecting long-ranged jumps, may be associated with superdiffusion. The term Lèvy flight is often used in this context, meaning that the jump length decays, asymptotically, as a power of the length, making thus possible for long jumps in a single step.

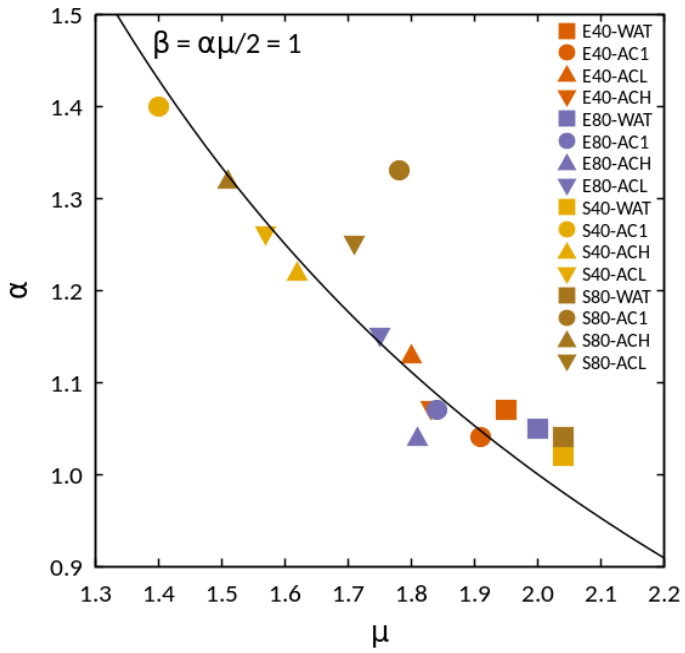

Fig. 8. Values of α and μ, obtained employing the q-scaling approach for all systems investigated. A black line, corresponding to the equation $\beta = 2\alpha\mu = 1$, has also been reported as a guide to the eye.

Based on this model, the actual value of α, as described by Eq. (11), reflects the competition between subdiffusion and superdiffusion (Yang, Reutens, & Vegh, 2022). In principle, different combinations of μ and β may eventually lead to the exact value of α. In practice, however, the spatial and temporal contributions in commonly observed subdiffusion and superdiffusion are often distinct, falling into two main categories, e.g. $\mu=2$ and $\beta<1$, and $\mu<2$ and $\beta=1$ (Palombo et al., 2011).

A similar consideration also applies to the species considered in this work. For example, figure 8 compares the values of μ and β for all the samples investigated. With few exceptions (S80-AC1 and S80-ACL), the samples closely approach the line corresponding to $\beta=1$. This excludes the

possibility of a time-fractional behaviour, supporting the idea that molecular transport within the hydrogel is essentially unrestricted for both compounds. This hypothesis is supported by the large difference between the hydrodynamics radii and the average mesh sizes (see above).

While CTRW provides an indispensable tool to decouple temporal and spatial contributions to the displacement distribution function, it also raises an important question about the origin of superdiffusion in S40 and S80 samples. Applying this theory of such samples entirely drops the deviations from the Fickian behaviour on the spatial domain ($\mu < 2$). According to this picture, salicylate molecules can be expected to perform occasionally long-range displacements while randomly diffusing within the hydrogel matrix. The origin of such long-ranged excursions does not have a clear interpretation within the CTRW framework and can hardly be explained considering the fitting of our data alone.

An alternative and perhaps, more compelling interpretation is offered by the random walk model proposed by Lutsko et al. (Lutsko, & Boon, 2013), where the diffusion regime is related to the mutual interactions between charged diffusing particles. According to this approach, subdiffusion can be observed when attractive interactions dominate particle diffusion. This may be the case with ionic liquids, for which subdiffusion has been observed on small time-scales (Casalegno et al., 2017).

Conversely, superdiffusion may settle in when repulsive interactions are dominant. Although our data do not allow for quantitative predictions, some qualitative considerations about the applicability of this model can be drawn, considering the chemical composition of our systems. In this respect, we notice that neat agarose-carbomer hydrogels (AC1) and those modified by reaction with the hyaluronic acid (ACH and ACL) display an anionic character in water. The same character is also found in sodium salicylate due to the presence of salicylate anion (pKa = 2.97, at 25°C)

(Wishart et al.) in water, whereas ethosuximide is a neutral molecule. Therefore, although both molecules may form hydrogen bonds with suitable functional groups in the hydrogel matrix, only salicylate can be expected to establish electrostatic interactions with the matrix. The fact that these interactions are essentially repulsive may provide an explanation of the observed superdiffusive behaviour.

3.4 Drug release kinetics

The drug release behaviour of the AC1 and AC-hyaluronic acid (ACL) hydrogels is investigated by loading small drugs, such as ethosuximide or sodium salicylate, in the hydrogel polymer matrix. The fractional mass release of ethosuximide from both hydrogels formulations is displayed in Figure 9. An initial *burst* effect (up to 30 min) is observed for AC1 (~25%) and ACL (~35%) respectively; after which a sustained release is observed for both formulations. The initial *burst* release is due to the motion of the drug located on the polymer surface or into the water-filled large pores, while the prolonged release is due to drug-polymer interactions that prevent the drug from passing into the release medium. The complete release of ethosuximide (~99%) is reached in 6-7 hours by ACL and AC1 hydrogels, respectively. A slightly faster release is observed for ethosuximide from ACL hydrogel formulation due to a larger mesh size of the polymer network.

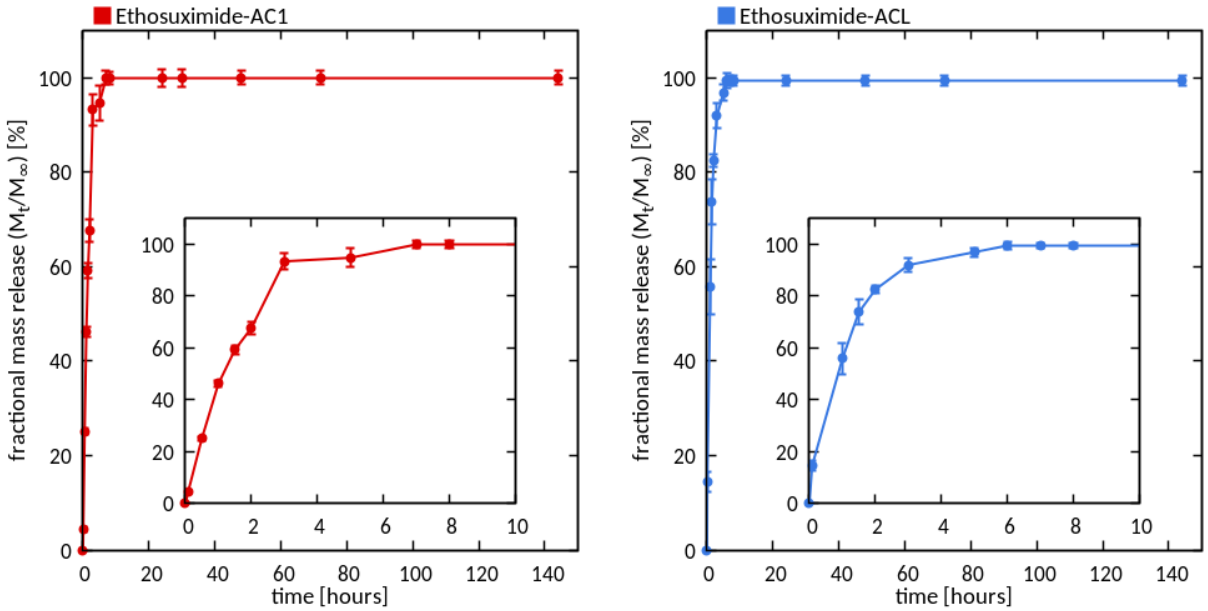

Fig. 9. Fractional mass release for ethosuximide samples from AC1 (*left*) and ACH (*right*) at 37° C. Details about initial (0-8) hours release behaviour are given in the insets.

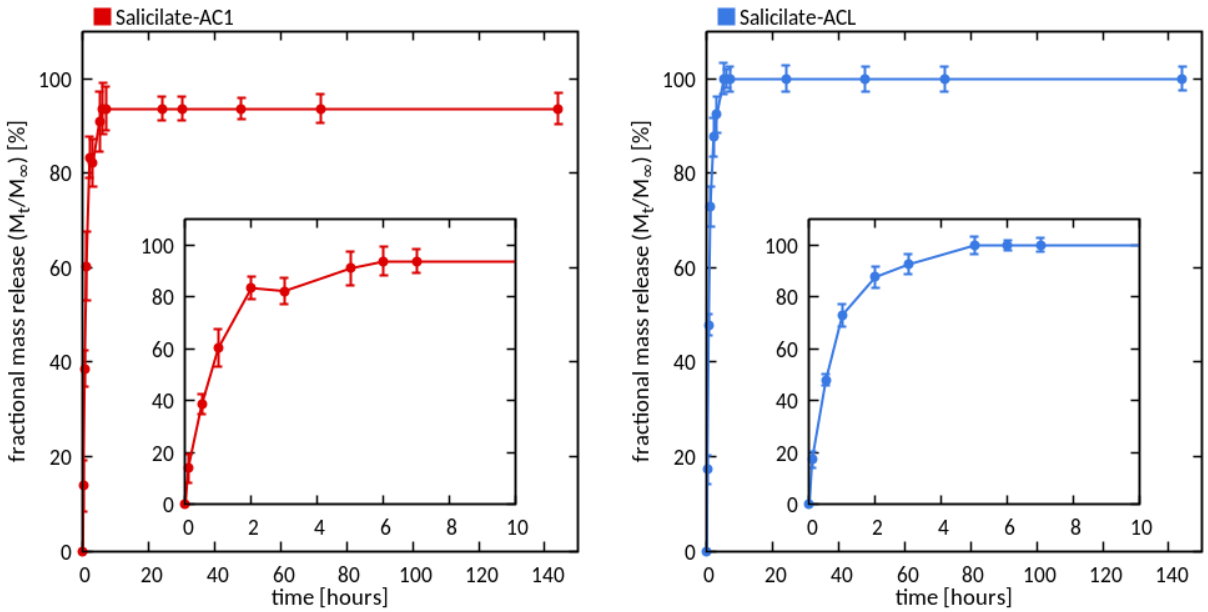

Fig. 10. Fractional mass release for sodium salicylate samples from AC1 (*left*) and ACL (*right*) at 37° C. Details about initial (0-8) hours release behaviour are given in the insets.

Similarly, the release profile of sodium salicylate from both hydrogel formulations (see Figure 10) show an initial *burst* effect, then a sustained release profile is observed until the entire amount of the drug (~99%) is released by the end of 5 hours from the ACL formulation, while ~93% of the drug is released in 6 hours from the AC1 hydrogel matrix. Overall, these results indicate that the structure of the hydrogel/mesh size and the presence of hyaluronic acid moiety impact the macroscopic drug release. Moreover, the net negative charge of the drug, in the case of sodium salicylate, imposes a superdiffusive motion regime in the microscopic time scale which is reflected in a faster macroscopic release of the drug from both hydrogel formulations.

3 Conclusions

This study investigated the diffusion regime of small drugs ethosuximide and sodium salicylate loaded in agarose-carbomer and hyaluronic acid-based hydrogel networks by ^{1}H HR-MAS NMR using the variable diffusion time approach.

Data analysis performed within the continuous time random walk theory suggests a superdiffusive motion for sodium salicylate molecules due to repulsive interactions between the drug (which has a negative net charge) and the anionic polymer matrix. The superdiffusive behaviour is retained in all hydrogel formulations regardless of the polymer mesh size and drug concentration, thus suggesting that drug-polymer electrostatic interactions may determine the type of motion. Conversely, the diffusion motion of ethosuximide - a neutral molecule - in AC1 and AC-HA hydrogels is unrestricted, similarly to that observed in water solution, while for the ACL sample, a mild superdiffusive behaviour is observed.

All the above results were made possible by developing a novel approach for determining the diffusion exponent based on the relationships between the direct and reciprocal representations of NMR signals. Comparing this method with standard regression indicates that the latter is inadequate to model diffusion in samples where deviations from unrestricted diffusion occur.

We believe this finding is necessary due to the increasing number of soft systems currently investigated employing NMR techniques, and the on-going debate on anomalous diffusion.

Our *in vitro* release studies showed sustained release of both drugs from AC1 and ACL formulations. In all formulations, the release kinetics of sodium salicylate is slightly faster in the hyaluronic acid-based hydrogel and always faster than the release profile of ethosuximide. We speculate that this outcome can be connected to the superdiffusion observed for sodium salicylate. Meanwhile, this work provides physico/chemical insights into the diffusivity of small drug molecules in hyaluronic-based hydrogel polymer networks. Finally, it demonstrates how the molecular motion and the macroscopic release process in anionic hydrogels can be related to the type of polymer units, polymer mesh size and net charge of the drugs. A fine-tuning of all these features allow us to optimise a drug delivery system.

Appendix A. Supplementary data

Supplementary data to this article can be found online.

References

Alam, T. M., Childress, K. K., Pastoor, K., Rice, C. V. (2014). Characterisation of Free, Restricted, and Entrapped Water Environmentsin Poly(N-isopropyl acrylamide) Hydrogels via ^{1}H HRMAS PFG NMR Spectroscopy. *Journal of Polymer Science, part B: Polymer Physics, 52,* 1521–1527.

Alvarez-Lorenzo, C., Blanco-Fernandez, B., Puga, A. M., Concheiro, A. (2013). Crosslinked ionic polysaccharides for stimuli-sensitive drug delivery. *Advanced Drug Delivery Reviews, 65,* 1148-1171.

An, Y., Gao, L., & Wang, T. (2020). Graphene oxide/alginate hydrogel fibers with hierarchically arranged helical structures for soft actuator application. *ACS Applied Nano Materials, 3*, 5079–5087.

Axpe, E., Chan, D., Offeddu, G. S., Chang, Y., Merida, D., Lopez Hernandez, H. and Appel, E. A. (2019). A Multi-scale Model for Solute Diffusion in Hydrogels. *Macromolecules, 52,* 6889-6897.

Burdick, J. A., & Prestwich, G. D. (2011). Hyaluronic acid hydrogels for biomedical applications. *Advanced Materials, 23,* H41–H56.

Blumen, A., Zumofen, G. and Klafter J. (1989). Transport aspects in anomalous diffusion: Lévy walks. *Phys. Rev. A, 40*, 3964-3973.

Capuani, S., Palombo, M., Gabrielli, A., Orlandi, A., Maraviglia, B., Pastore, F. S. (2013). Spatio-temporal anomalous diffusion imaging: results in controlled phantoms and in excised human meningiomas. *Magn. Reson. Imaging, 31 (3),* 359–365.

Casalegno, M., Raos, G., Appetecchi, G.B., Passerini, S., Castiglione, F., Mele, A. (2017). From nanoscale to microscale: crossover in the diffusion dynamics within two pyrrolidinium-based ionic liquids. *Journal of Phys. Chem. Lett., 8,* 5196-5202.

Castiglione, F., Casalegno, M., Ferro, M., Rossi, F., Raos, G. and Mele A. (2019). Evidence of superdiffusive nanoscale motion in anionic polymeric hydrogels: Analysis of PGSE- NMR data and comparison with drug release properties. *J Controlled Release, 305*, 110-119.

Chen, T., Liu, H., Dong, C., An, Y., Liu, J., Li, J., Li, X., Si, C., Zhang, M. (2020). Synthesis and characterisation of temperature/pH dual sensitive hemicellulose-based hydrogels from eucalyptus APMP waste liquor. *Carbohydrate Polymers, 247,* Article 116717.

Cohen, Y. and Assaf, Y. (2002). High *b*-value q-space analysed diffusion-weighted MRS and MRI in neuronal tissues – a technical review. *NMR Biomed., 15*, 516-542.

Cuetos, A., Morillo N. and Patti A. (2018). Fickian yet non-Gaussian diffusion is not ubiquitous in soft matter. *Phys. Rev. E, 98,* Article 042129.

Cukier, R. I. (1984). Diffusion of Brownian spheres in semidilute polymer solutions. *Macromolecules, 17*, 252-255.

Di Meo, C., Coviello, T., Matricardi, P., Lamanna, R. (2021). Anomalous Enhanced Water Diffusion in Polysaccharide Interpenetrating Hydrogels. *Colloids Surfaces A Physicochem. Engineering Aspects, 613*, 125892.

Elvira, C., Mano, J. F., San Román, J., Reis, R. L. (2002). Starch-based biodegradable hydrogels with potential biomedical applications as drug delivery systems. *Biomaterials 23*, 1955−1966.

Ferro, M., Castiglione, F., Punta, C., Melone, L., Panzeri, W., Rossi, B., Trotta, F. and Mele A. (2014). Anomalous diffusion of Ibuprofen in cyclodextrin nanosponges hydrogels: an HRMAS NMR study. *Beilstein J. Org. Chem., 10*, 2580-2593.

Fick, A. (1855). Ueber Diffusion. *Ann. Phys., 170,* 59-86.

Fujita, H. (1961). Diffusion in polymer-diluent systems. *Adv. Polym. Sci. 3*, 1-47.

Garg, H. G. and Hales, C. A. (2004). Chemistry and Biology of Hyaluronan, Elsevier Ltd., Oxford.

Hacker, M.C., Nawaz, H.A. (2015). Multi-functional macromers for hydrogel design in biomedical engineering and regenerative medicine. *Int. J. Mol. Sci. 16*, 27677-27706.

Hamedi, H., Moradi, S., Hudson, S. M., Tonelli, A. E. (2018). Chitosan based hydrogels and their applications for drug delivery in wound dressings: A review. *Carbohydrate Polymers, 199*, 445–460.

Jayakumar, A., Jose, V. K. and Lee, J.-M. (2020). Hydrogels for medical and environmental applications. *Small Methods, 4*, 1900735.

Jenkins, J. E., Hibbs, M. R. and Alam, T. M. (2012). Identification of Multiple Diffusion Rates in Mixed Solvent Anion Exchange Membranes Using High Resolution MAS NMR. *ACS Macro Lett., 1*, 910-914.

Johnson, C.S. (1999). Diffusion ordered nuclear magnetic resonance spectroscopy: principles and applications. *Prog. Nucl. Magn. Reson. Spec. 34*, 203-256.

Kasula, N., Madhusudana, R. K., Krishna, R. K.S.V., Soo, H. S. (2022). Dual responsive tamarind gum-co-poly(N-isopropyl acrylamide-co-ethylene glycol vinyl ether) hydrogel: A promising device for colon specific anti-cancer drug delivery. *Colloids and Surfaces A: Physicochemical and Engineering Aspects, 641*,128456.

Kusumi, A., Tsunoyama, T. A., Hirosawa, K. M., Kasai, R. S., Fujiwara, T. K. (2014). Tracking single molecules at work in living cells. *Nat. Chem. Biol., 10,* 524-532.

Kwon, S.S., Kong B.J. and Park, S.N. (2015). Physicochemical properties of pH-sensitive hydrogels based on hydroxyethyl cellulose–hyaluronic acid and for applications as transdermal delivery systems for skin lesions. *Eur. J. Pharm. Biopharm., 92*, 146-154.

Ikeda, M., Ochi, R., Wada, A., Hamachi, I. (2010). Supramolecular hydrogel capsule showing prostate specific antigen-responsive function for sensing and targeting prostate cancer cells. *Chemical Science, 1 (4),* 491-498.

Laurent, T. C. E. (1998). The Chemistry, Biology, and Medical Applications of Hyaluronan and its Derivatives, Portland Press, Miami.

Levenberg, K. (1944). A method for the solution of certain non-linear problems in least squares. *Quarterly of Applied Mathematics, 2 (2),* 164-168.

Liang, S., Xu, J., Weng, L., Dai, H., Zhang X. and Zhang, L. (2006). Protein diffusion in agarose hydrogel in situ measured by improved refractive index method. *J. Controlled Release*, *115*, 189-196.

Liao, J. and Huang, H. (202). Review on magnetic natural polymer constructed hydrogels as vehicles for drug delivery. *Biomacromolecules, 21*, 2574−2594.

Lin, G. (2017). Analysing signal attenuation in PFG anomalous diffusion via a modified Gaussian phase distribution approximation based on fractal derivative model. *Physica A 467,* 277–288.

Liu, Z., Jiao, Y., Wang, Y., Zhou, C., Zhang, Z. (2008). Polysaccharides-based nanoparticles as drug delivery systems. *Adv. Drug Deliv. Rev. 60*, 1650–1662.

Loebel, C., Rodell C. B., Chen, M. H., Burdick, J. A. (2017). Shear-thinning and self-healing hydrogels as injectable therapeutics and for 3Dprinting. *Nat. Protoc*. *12*, 1521-1541.

Lutsko, J. F., Boon, J. P. (2013). Microscopic Theory of Anomalous Diffusion Based on Particle Interactions. *Phys. Rev. E, 88 (2),* 1-8.

Malgaretti, P., Pagonabarraga, I., Miguel Rubi, J. (2016). Rectification and non-gaussian diffusion in heterogeneous media. *Entropy, 18 (11),* 1–12.

Masaro, L., Zhu, X. X. L. (1999). Physical models of diffusion for polymer solutions, gels and solids. *Prog. Polym. Sci. 24*, 731-775.

Metzler, R., Klafter, J. (2000). The Random Walk's Guide to Anomalous Diffusion: A Fractional Dynamics Approach. *Phys. Rep*., *339 (1)*, 1-77.

Michalik, R. and Wandzik I. (2020). A mini-review on chitosan-based hydrogels with potential for sustainable agricultural applications. *Polymers, 12*, 2425.

Omidi, S., Pirhayati, M., Kakanejadifard, A. (2020).Co-delivery of doxorubicin and curcumin by a pH-sensitive, injectable, and in situ hydrogel composed of chitosan, graphene, and cellulose nanowhisker. *Carbohydrate Polymers, 231*, Article 115745.

Palombo, M., Barbetta, A., Cametti, C., Favero, G., Capuani, S. (2022). Transient anomalous diffusion MRI measurement discriminates porous polymeric matrices characterised by different sub-microstructures and fractal dimension. *Gels 2022, 8*, 95.

Palombo, M., Gabrielli, A., De Santis, S., Cametti, C., Ruocco, G., Capuani, S. (2011). Spatio-temporal anomalous diffusion in heterogeneous media by nuclear magnetic resonance. *J. Chem. Phys.*, *135 (3)*, 034504.

Perale, G., Rossi, F., Santoro, M., Marchetti, P., Mele, A., Castiglione, F., Raffa, E., Masi, M. (2011). Drug release from hydrogel: a new understanding of transport phenomena, *J. Biomed. Nanotechnol., 7*, 476-481.

Pivato, V. R., Rossi, F., Ferro, M., Trotta, F., Castiglione, F. and Mele, A. (2021). β-cyclodextrin nanosponge hydrogels as drug delivery nanoarchitectonics for multistep drug release kinetics. *ACS Appl. Polym. Mater., 3*, 6562–6571.

Pizzetti, F., Maspes, A., Rossetti, A., Rossi, F. (2021). The addition of hyaluronic acid in chemical hydrogels can tune the physical properties and degradability. *European Polymer Journal, 161,* 110843.

Rial-Hermida, M. I., Rey-Rico, A., Blanco-Fernandez, B., Carballo-Pedrares, N., Byrne, E. M. and Mano, J. F. (2021). Recent progress on polysaccharide-based hydrogels for controlled delivery of therapeutic biomolecules. *ACS Biomater. Sci. Eng*., *7*, 4102-4127.

Rossi, F., Castiglione, F., Ferro, M., Marchini, P., Mauri, E., Moioli, M., Mele, A., and Masi, M. (2015). Drug–polymer interactions in hydrogel-based drug-delivery systems: an experimental and theoretical study. *Chem. Phys. Chem., 16,* 2818 – 2825.

Sagi, Y., Brook, M., Almog, I., Davidson, N. (2012). Observation of Anomalous Diffusion and Fractional Self-Similarity in One Dimension. *Phys. Rev. Lett., 108,* Article 093002.

Schanté, C. E., Zuber, G., Herlin, C., & Vandamme, T. F. (2011). Chemical modifications of hyaluronic acid for the synthesis of derivatives for a broad range of biomedical applications. *Carbohydrate Polymers, 85*, 469–489.

Serag, M. F., Abadi, M. & Habuchi, S. (2014). Single-molecule diffusion and conformational dynamics by spatial integration of temporal fluctuations. *Nature Communications, 6*, Article 5123.

Shelke, N.B., James, R., Laurencin, C.T., Kumbar, S.G. (2014). Polysaccharide biomaterials for drug delivery and regenerative engineering. *Polym. Adv. Technol*. *25*, 448-460.

Song, M. S., Moon, H. C., Jeon, J. H., Park, H. Y. (2018). Neuronal Messenger Ribonucleoprotein Transport Follows an Aging Lévy Walk. *Nature Communications, 9 (1),* 1–8.

Tokuyama, H., Nakahata, Y., Ban, T. (2020). Diffusion coefficient of solute in heterogeneous and macroporous hydrogels and its correlation with the effective crosslinking density. *Journal of Membrane Science, 595,* 117533.

Viswanathan, G. M., Afanasyev, V., Buldyrev, S. V., Murphy, E. J., Prince, P. A., Stanley, H. E. (1996). Lévy Flight Search Patterns of Wandering Albatrosses. *Nature, 381 (6581)*, 413-415.

Wang, Y., Garcia, C. R., Ding, Z., Gabrilska, R., Rumbaugh, K. P., Wu, J., Liu, Q., Li, W. (2020). Adhesive, self-healing, and antibacterial chitosan hydrogels with tunable two-layer structures. *ACS Sustainable Chemistry & Engineering, 8(49),* 18006–18014.

Wang, B., Kuo, J., Bae, S. C., Granick, S. (2012). When Brownian diffusion is not Gaussian. *Nature Materilas, 11*, 481–485.

Wang, B., Anthony, S. M., Sung, C. B., Granick, S. (2009). Anomalous yet Brownian. *Proc. Natl. Acad. Sci. U. S. A., 106* (36), 15160-15164.

Wishart, D. S., Djombou Feunang, Y., Guo, A. C., Lo, E. J., Marcu, A., Grant, J. R., Sajed, T., Johnson, D., Li, C., Sayeeda, Z., Assempour, N., Iynkkaran. I., Liu, Y., Maciejewski, A., Gale, N., Wilson, A., Chin, L., Cummings, R., Le, D., Pon, A., Knox, C., Wilson, M. "Salycylic acid | DrugBank Online". DrugBank. 5.0.

Xiao, R., Grinsta, M.W. (2017). Chemical synthesis of polysaccharides and polysaccharide mimetics. *Prog. Polym. Sci*. *74*, 78-116.

Xue, X., Hu, Y., Deng, Y., Su, J. (2021). Recent Advances in Design of Functional Biocompatible Hydrogels for Bone Tissue Engineering. *Adv. Funct. Mater. 31,* 2009432.

Xu, K., Yao, H., Fan, D., Zhou, L., Wei, S. (2021). Hyaluronic acid thiol modified injectable hydrogel: synthesis, characterisation, drug release, cellular drug uptake and anticancer activity. *Carbohydrate Polymers, 254,* Article 117286.

Yang, Q., Reutens, D. C., Vegh, V. (2021). Generalisation of continuous time random walk to anomalous diffusion MRI models with an age-related evaluation of human corpus callosum. *Neuroimage, 250,* 118903.

Yongyan, Y., Lifeng, X., Jingfei, W., Qingye, M., Shuangling, Z., Yan, G., Xuejun, C. (2022). Recent advances in polysaccharide-based self-healing hydrogels for biomedical applications. *Carbohydrate Polymers, 283,* Article 119161.

Zarrintaj, P., Manouchehri, S., Ahmadi, Z., Saeb, M. R., Urbanska, A. M., Kaplan, D. L., Mozafari, M. (2018). Agarose-based biomaterials for tissue engineering. *Carbohydrate Polymers, 187,* 66-84.

Zubkov, M., Dennis, G. R., Stait-Gardner, T., Torres, A. M., Willis, S. A., Zheng, G. and Price, W. S. (2016). Physical characterisation using diffusion NMR Spectroscopy. *Magn. Reson. Chem., 55,* 414-424.

Zustiak, S.P., Boukari, H., Leach, J.B. (2010). Solute diffusion and interactions in cross-linked poly(ethylene glycol) hydrogels studied by fluorescence correlation spectroscopy. *Soft Matter, 6,* 3609-3618.